Two-body D_s^+ decays to $\eta\pi^+$, $\eta'\pi^+$, $\eta\rho^+$, $\eta'\rho^+$, and $\phi\rho^+$

M. Daoudi,[a] W. T. Ford,[a] D. R. Johnson,[a] K. Lingel,[a] M. Lohner,[a] P. Rankin,[a]
J. G. Smith,[a] J. Alexander,[b] C. Bebek,[b] K. Berkelman,[b] D. Besson,[b] T. E. Browder,[b] D. G. Cassel,[b]
E. Cheu,[b] D. M. Coffman,[b] P. S. Drell,[b] R. Ehrlich,[b] R. S. Galik,[b] M. Garcia-Sciveres,[b] B. Geiser,[b]
B. Gittelman,[b] S. W. Gray,[b] D. L. Hartill,[b] B. K. Heltsley,[b] K. Honscheid,[b] J. Kandaswamy,[b] N. Katayama,[b]
P. C. Kim,[b] D. L. Kreinick,[b] J. D. Lewis,[b] G. S. Ludwig,[b] J. Masui,[b] J. Mevissen,[b] N. B. Mistry,[b]
S. Nandi,[b] C. R. Ng,[b] E. Nordberg,[b] C. O'Grady,[b] J. R. Patterson,[b] D. Peterson,[b] M. Pisharody,[b]
D. Riley,[b] M. Sapper,[b] M. Selen,[b] H. Worden,[b] M. Worris,[b] P. Avery,[c] A. Freyberger,[c]
J. Rodriguez,[c] J. Yelton,[c] S. Henderson,[d] K. Kinoshita,[d] F. Pipkin,[d] M. Saulnier,[d] R. Wilson,[d]
J. Wolinski,[d] D. Xiao,[d] H. Yamamoto,[d] A. J. Sadoff,[e] R. Ammar,[f] P. Baringer,[f] D. Coppage,[f]
R. Davis,[f] M. Kelly,[f] N. Kwak,[f] H. Lam,[f] S. Ro,[f] Y. Kubota,[g] J. K. Nelson,[g]
D. Perticone,[g] R. Poling,[g] S. Schrenk,[g] M. S. Alam,[h] I. J. Kim,[h] B. Nemati,[h] V. Romero,[h]
C. R. Sun,[h] P.-N. Wang,[h] M. M. Zoeller,[h] G. Crawford,[i] R. Fulton,[i] K. K. Gan,[i] T. Jensen,[i]
H. Kagan,[i] R. Kass,[i] R. Malchow,[i] F. Morrow,[i] J. Whitmore,[i] P. Wilson,[i] F. Butler,[j]
X. Fu,[j] G. Kalbfleisch,[j] M. Lambrecht,[j] P. Skubic,[j] J. Snow,[j] P.-L. Wang,[j] D. Bortoletto,[k]
D. N. Brown,[k] J. Dominick,[k] R. L. McIlwain,[k] D. H. Miller,[k] M. Modesitt,[k] E. I. Shibata,[k] S. F. Schaffner,[k]
I. P. J. Shipsey,[k] M. Battle,[l] J. Ernst,[l] H. Kroha,[l] S. Roberts,[l] K. Sparks,[l] E. H. Thorndike,[l]
C.-H. Wang,[l] M. Artuso,[m] M. Goldberg,[m] T. Haupt,[m] N. Horwitz,[m] R. Kennett,[m] M. D. Mestayer,[m]
G. C. Moneti,[m] Y. Rozen,[m] P. Rubin,[m] T. Skwarnicki,[m] S. Stone,[m] M. Thusalidas,[m] W.-M. Yao,[m]
G. Zhu,[m] A. V. Barnes,[n] J. Bartelt,[n] S. E. Csorna,[n] V. Jain,[n] T. Letson,[n] D. S. Akerib,[o]
B. Barish,[o] D. F. Cowen,[o] G. Eigen,[o] R. Stroynowski,[o] J. Urheim,[o] A. J. Weinstein,[o] R. J. Morrison,[p]
H. Tajima,[p] D. Schmidt,[p] and M. Procario[q]

(CLEO Collaboration)

[a]*University of Colorado, Boulder, Colorado 80309-0390.*
[b]*Cornell University, Ithaca, New York 14853.*
[c]*University of Florida, Gainesville, Florida 32611.*
[d]*Harvard University, Cambridge, Massachusetts 02138.*
[e]*Ithaca College, Ithaca, New York 14850.*
[f]*University of Kansas, Lawrence, Kansas 66045*
[g]*University of Minnesota, Minneapolis, Minnesota 55455*
[h]*State University of New York at Albany, Albany, New York 12222*
[i]*Ohio State University, Columbus, Ohio, 43210*
[j]*University of Oklahoma, Norman, Oklahoma 73019*
[k]*Purdue University, West Lafayette, Indiana 47907*
[l]*University of Rochester, Rochester, New York 14627*
[m]*Syracuse University, Syracuse, New York 13244*
[n]*Vanderbilt University, Nashville, Tennessee 37235*
[o]*California Institute of Technology, Pasadena, California 91125*
[p]*University of California at Santa Barbara, Santa Barbara, California 93106*
[q]*Carnegie-Mellon University, Pittsburgh, Pennsylvania, 15213*

(Received 30 September 1991)

We have made measurements of several D_s branching ratios, relative to the $\phi\pi^+$ mode. We have observed two previously unseen two-body hadronic decays of the D_s^+, namely $\eta\rho^+$ and $\eta'\rho^+$, and measured relative branching ratios of $2.86\pm0.38^{+0.36}_{-0.38}$ and $3.44\pm0.62^{+0.44}_{-0.46}$, respectively. We have determined the relative branching ratio for the decay into $\phi\rho^+$ to be $1.86\pm0.26^{+0.29}_{-0.40}$. In addition, we have measured relative branching ratios for the $\eta\pi^+$ and $\eta'\pi^+$ states, for which there had previously been conflicting measurements; our results are $0.54\pm0.09\pm0.06$ and $1.20\pm0.15\pm0.11$, respectively. Combining these new measurements with previous results and using $(3.7\pm1.2)\%$ for the value of $\mathcal{B}(D_s\to\phi\pi^+)$, we can account for $\approx(79\pm26)\%$ of all D_s^+ decays. In addition we have also measured relative branching ratios or set upper limits on D^+ decays to all of the above-mentioned final states.

PACS number(s): 13.25.+m, 14.40.Jz

I. INTRODUCTION

D_s^+ was first observed in the $\phi\pi^+$ decay mode [1]. Since then a number of other hadronic decay modes have been found [2] and $D_s^+\to\phi l^+\nu$ has been seen [3,4]. Prior to this work, the major portion of D_s decays was unknown, leading to speculation that there existed some unobserved, but rather large, two-body decay modes.

There were also inconsistent measurements of the branching ratios for the $\eta\pi^+$ and $\eta'\pi^+$ modes. In this paper we present new measurements of the decay branching ratios for these modes and report measurements of the previously unseen modes $\eta\rho^+$ and $\eta'\rho^+$ as well as the previously observed $\phi\rho^+$ mode. We compare our measurements with theoretical predictions and, finally, summarize what is known about D_s decay branching fractions.

The data were collected with the CLEO II detector at the Cornell Electron Storate Ring (CESR). We use a total of 689 pb^{-1} from the $\Upsilon(3S)$ and $\Upsilon(4S)$ resonances and from e^+e^- center-of-mass energies just below and above the $\Upsilon(4S)$ resonance.

The CLEO II detector is designed to detect both charged and neutral particles with high resolution and efficiency. The detector consists of a charged-particle tracking system surrounded by a time-of-flight scintillation system and an electromagnetic shower detector consisting of 7800 Tl-doped CsI crystals [5]. The tracking system, the time-of-flight system, and the calorimeter are installed inside a 1.5-T superconducting coil. Muon detection is achieved using proportional tubes interleaved with iron. A more detailed description of the detector can be found elsewhere [6].

In this analysis, only photon candidates in the barrel region of the detector are used, i.e., $|\cos\theta| < 0.7$, where θ is the angle with respect to the beam direction. The barrel region has less material in front of the CsI crystals than other areas of the detector. Each neutral energy cluster is required to have at least 30 MeV of energy and not match to a charged track projected into the calorimeter. Charged tracks were required to have measured ionization losses (dE/dx) consistent within 2.5 standard deviations of that expected for the particular hypothesis under consideration. All D_s candidates are required to have $x = P_{D_s}/E_{\text{beam}} > 0.567$ (approximately 3 GeV/c), in order to reduce background mass combinations. To remove background from $\Upsilon(3S)$ resonant events, we require that the ratio of Fox-Wolfram moments, H_2/H_0, be greater than 0.2 for this portion of the data sample [7]. Whenever a specific state or decay mode is mentioned in this work, the charge-conjugate state or decay mode is always included in the analysis.

In this paper, we concentrate on decay modes which can be explained as occurring via a simple spectator diagram where the c quark decays into an s quark plus a virtual W^+, and the resulting $s\bar{s}$ system forms a single meson, either a ϕ, η, or η', and the virtual W^+ materializes as either a π^+ or a ρ^+.

II. SELECTION OF ϕ, η, AND η'

The K^+K^- invariant-mass distribution for all K^+K^- momenta is shown in Fig. 1. There is a clear peak at the ϕ mass. The fit to a Breit-Wigner resonance formula, shown in the figure, gives a mass resolution of 7.2 MeV full width at half maximum (FWHM). This fit contains contributions from both the detector resolution and the natural width of the resonance.

The η is detected in the decay modes, $\gamma\gamma$ and $\pi^+\pi^-\pi^0$,

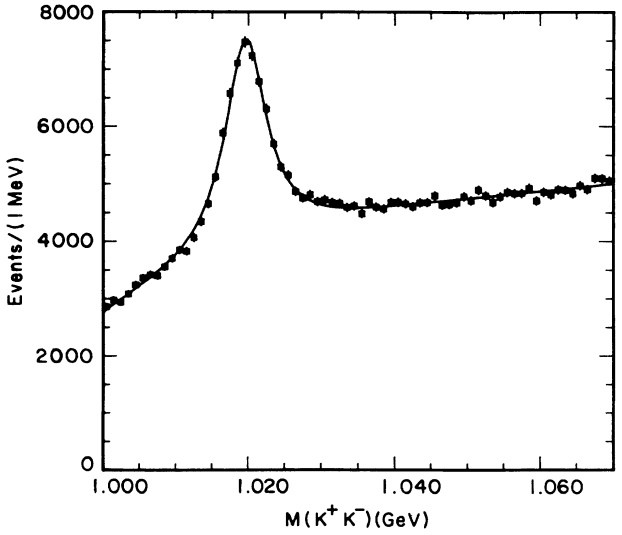

FIG. 1. The K^+K^- invariant-mass distribution.

for which the branching ratios are 38.9% and 23.6%, respectively [2]. The $\gamma\gamma$ invariant-mass distribution for momenta above 1.5 GeV/c is shown as the histogram in Fig. 2(a). We also require that the decay angle cosine between both of the γ's and the $\gamma\gamma$ direction in the laboratory transformed into the $\gamma\gamma$ rest frame be smaller than 0.8. There is considerable background, mostly from π^0 decays. When we eliminate any photon which, with another photon, makes a mass combination such that the combination is consistent with π^0 mass and has a π^0 momentum in excess of 0.8 GeV/c, we are left with the η signal shown as the solid points. Monte Carlo simula-

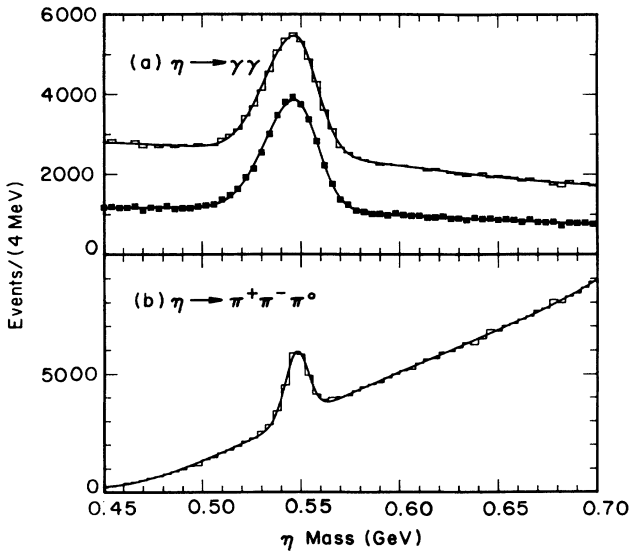

FIG. 2. (a) The $\gamma\gamma$ invariant-mass distribution for $\gamma\gamma$ momenta above 1.5 GeV/c (histogram). Removing π^0 candidates with momenta above 0.8 GeV/c produces the distribution shown with solid points. (b) The $\pi^+\pi^-\pi^0$ invariant-mass distribution for candidate momenta above 1.5 GeV/c.

tions show that this procedure keeps 92% of the η's and reduces the background by 50%. The fitted η width is 14 MeV (rms).

Turning now to the other η decay model used, we show the $\pi^+\pi^-\pi^0$ mass distribution in Fig. 2(b) for candidate momenta above 1.5 GeV/c. All neutral-pion candidates in this paper are selected by requiring that the $\gamma\gamma$ invariant mass be consistent with the known π^0 mass within 2.5 times the rms width. In addition we impose the same decay angle requirement as we did on the $\eta\to\gamma\gamma$ decay. A kinematic fit was then made using the π^0 mass as a constraint and adjusting the measured energies and angles. In the subsequent analysis we use the resulting fitted quantities. In addition, we required that the π^0 momentum be greater than 0.3 GeV/c. A clear signal is visible at the η mass, with fitted width of 6.0 MeV (rms). (The cut, requiring the momenta of the combinations, shown in Fig. 2, to be greater than 1.5 GeV/c, was used only to display the η signal, but is not retained in the subsequent analysis.)

The η' is detected in the decay modes $\pi^+\pi^-\eta$ and $\rho^0\gamma$ for which the branching ratios are 44.2% and 30.0%, respectively [2]. We require that the η momentum be larger than 0.3 GeV/c to suppress background. To select $\rho^0\gamma$ candidates, we require the γ momentum be above 0.1 GeV/c and that the $\pi^+\pi^-$ be consistent with the ρ^0 mass. Because of the limited phase space for the ρ in this decay, the $\pi^+\pi^-$ mass spectrum is modified in shape [8]. We require $0.85 > M_{\pi^+\pi^-} > 0.50$ GeV, which has an acceptance of 92%. Since the γ cannot have a transverse spin component, the ρ is polarized as $\sin^2\theta_{\pi^+}$, where θ_{π^+} is the angle between the π^+ direction and the photon direction in the ρ^0 rest frame. To optimize the signal-to-background ratio we require that $|\cos\theta_{\pi^+}| < 0.8$.

The mass plots for η' final states are shown in Fig. 3 where the candidate momenta are required to be above 1.5 GeV/c. In Fig. 3(a) only the $\eta\to\gamma\gamma$ component is included. The fitted η' widths for the two channels are 5.0 and 11.0 MeV (rms), respectively. The raw signal in the $\rho^0\gamma$ channel [Fig. 3(b)] does not stand out strongly, because it is superimposed on a large background caused, in part, by the large width of the ρ^0. (Again, the momentum cut, $p_{\eta'} > 1.5$ GeV/c, is not retained in the subsequent analysis.)

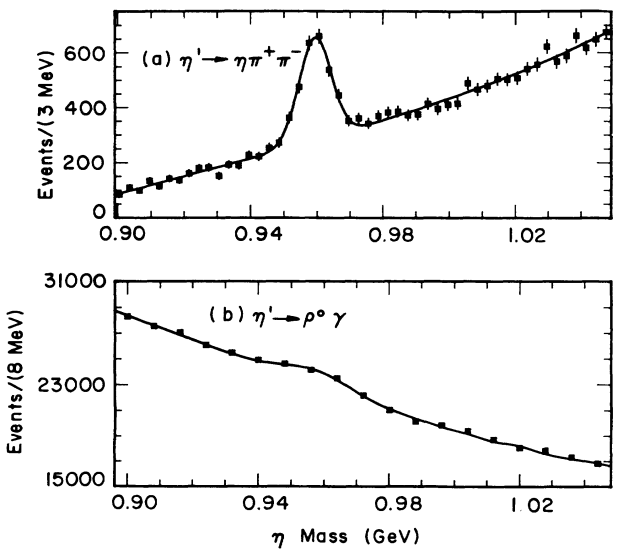

FIG. 3. (a) The $\eta\pi^+\pi^-$ invariant-mass plot for candidate momenta above 1.5 GeV/c, for the case $\eta\to\gamma\gamma$. (b) The $\rho^0\gamma$ invariant-mass plot for candidate momenta above 1.5 GeV/c.

III. DECAY MODES OF THE D_s^+ CONTAINING $A\pi^+$

A. Detection of the $\phi\pi^+$ mode

After selecting ϕ mesons within ± 8 MeV of the peak mass, we form the $\phi\pi^+$ mass spectrum shown in Fig. 4. There are two additional restrictions imposed on the data. Since the D_s has spin zero, the angular distribution of the ϕ in the D_s rest frame with respect to D_s direction must be uniform. The background tends to peak in the forward direction (in other decay modes also in the backward direction) and we require the cosine of this "decay angle," $\cos\alpha_\phi$, to be less than 0.8. In addition, this decay involves a spin-zero particle decaying into a spin-one ϕ and a spin-zero π. Thus the ϕ must be polarized in the helicity-zero state, giving a $\cos^2\theta_{K^+}$ distribution to the kaons, where θ_{K^+} is the angle between the K^+ and the D_s in the ϕ rest frame. We require $|\cos\theta_{K^+}| > 0.45$. There are two clear peaks in the mass distribution, one from D_s decay and the other from D^+ decay. We find 453 ± 28 D_s decays in this mode. In this fit to the D_s decay state and in all subsequent fits presented in this paper, the mass of the D_s was constrained to the accepted value of 1969 MeV and the width was constrained to the value determined from Monte Carlo simulations. Selection criteria for this mode and modes subsequently discussed are given in Appendix A.

We use this mode as the scale to which we normalize all the other D_s decay branching ratios measured in this paper. We also quote results for D^+ decays; however, in this case we normalize to our measurement of the $K^-\pi^+\pi^+$ channel. We find 5378 $K^-\pi^+\pi^+$ events and estimate our detection efficiency to be 50%. (Note that

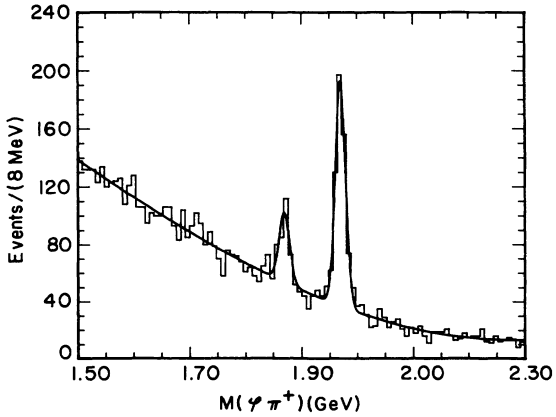

FIG. 4. The $\phi\pi^+$ invariant-mass spectrum.

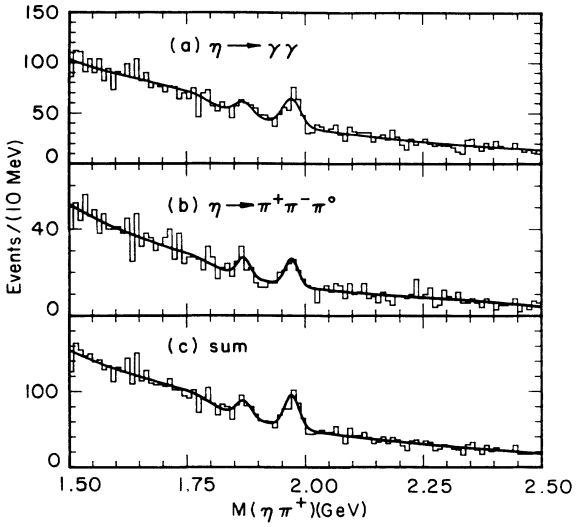

FIG. 5. The $\eta\pi^+$ invariant-mass spectrum using (a) the $\eta\rightarrow\gamma\gamma$ decay mode, and (b) the $\eta\rightarrow\pi^+\pi^-\pi^0$ decay mode; (c) the sum of the two modes. The fit is described in the text.

the efficiencies for D^+ are the same as for D_s^+ to the same final state.)

The relative branching ratio result is presented in Table II. This D^+ decay mode has been reported previously by several groups [2].

B. Detection of the $\eta\pi^+$ mode

In Fig. 5 we show the $\eta\pi^+$ invariant-mass spectrum for both η decay modes. The selection criteria are given in Appendix A. In the case of the $\pi^+\pi^-\pi^0$ decay mode, we required that the π^0 momentum be greater than 0.3 GeV/c to reduce background from slow π^0's. The fit to this mass spectrum includes a peak at the D^+ mass and the reflection from the decay $D_s^+\rightarrow\eta\rho^+$. In the latter decay mode, ρ^+ is fully polarized and the $\eta\pi^+$ submass reflects into an approximately 150-MeV-wide region. The shape of the latter contribution is obtained from Monte Carlo studies and the size determined from the branching ratio, presented subsequently in this paper. We also fitted the data with a Gaussian signal function of fixed mass and width, the latter determined from Monte Carlo studies, together with a third-order polynomial background. For the latter fit, a 150-MeV-wide region is excluded from the fit because of possible contamination from $D^+\rightarrow\eta\pi^+$ decay and from $D_s^+\rightarrow\eta\rho^+$ decay. We found that the number of decays obtained in the mode $D_s^+\rightarrow\eta\pi^+$ is the same within 5% for both fits discussed above. The number of D_s events is listed in Table I. To find a branching ratio relative to the $\phi\pi^+$ mode, efficiencies for the two modes were obtained from Monte Carlo simulations; the products of the efficiency times branching ratio for the daughter decays are also listed in Table I. We have performed checks on the efficiencies of the Monte Carlo simulations: these are summarized in Appendix B. Averaging over the two η decay modes, we find $\Gamma(D_s\rightarrow\eta\pi^+)/\Gamma(D_s\rightarrow\phi\pi^+)=0.54\pm0.09\pm0.04$. The first error is statistical and the second systematic. (Whenever two errors are quoted we follow this convention.) The systematic errors for the efficiencies relative to the $\phi\pi^+$ mode have several sources and differ slightly from mode to mode. For the $\eta\pi^+$ mode with the subsequent decay of the $\eta\rightarrow\gamma\gamma$ the systematic error includes uncertainties from fitting the $\eta\pi^+$ mass spectrum (6%), uncertainties in the relative charged track (4%) and photon detection efficiencies(5%), statistics from the Monte Carlo simulation (4.3%), uncertainties in the relative hadronic event-selection efficiencies (5%), and uncertainties in the π^0 veto efficiency (3%). The total systematic error is obtained by adding these uncorrelated errors in quadrature and is estimated to be $\pm12\%$.

The number of events found in the $D^+\rightarrow\eta\pi^+$ channel are 66.3 ± 25.5 and 32.7 ± 12.8 in the $\eta\rightarrow\gamma\gamma$ and $\pi^+\pi^-\pi^0$ channels, respectively. The sum of the two modes has a statistical significance of 3.6 standard deviations. We find a relative branching ratio for this decay which is listed in Table II.

TABLE I. Relative branching ratios for D_s modes.

Mode	$s\bar{s}$ decay	No. of events	Monte Carlo width (MeV)	$\epsilon\mathcal{B}$[a] (%)	$\Gamma/\Gamma(\phi\pi^+)$
$\phi\pi^+$	$\phi\rightarrow K^+K^-$	453±28	8.7	17.0	1
$\eta\pi^+$	$\eta\rightarrow\gamma\gamma$	123±24	19	8.17	0.56±0.11±0.07
	$\eta\rightarrow\pi^+\pi^-\pi^0$	42±12	14	3.14	0.49±0.15±0.07
$\eta'\pi^+$	$\eta'\rightarrow\eta\pi^+\pi^-$[b]	59±11	13	2.05	1.10±0.21±0.12
	$\eta'\rightarrow\rho^0\gamma$	200±34	11	5.40	1.38±0.25±0.20
	$\eta'\rightarrow\eta\pi^+\pi^-$[c]	22±7	12	0.75	1.12±0.36±0.15
$\eta\rho^+$	$\eta\rightarrow\gamma\gamma$	158±22	20	2.02	2.93±0.45±0.39
	$\eta\rightarrow\pi^+\pi^-\pi^0$	59±15	20	0.82	2.70±0.68±0.38
$\eta'\rho^+$	$\eta'\rightarrow\eta\pi^+\pi^-$[b]	53±10	20	0.56	3.55±0.71±0.53
	$\eta'\rightarrow\eta\pi^+\pi^-$[c]	15±6	20	0.18	3.10±1.24±0.45
$\phi\rho^+$	$\phi\rightarrow K^+K^-$	253±32	13	5.10	1.86±0.26±0.29

[a] ϵ, acceptance; $\mathcal{B}$, branching ratio of D_s daughters.
[b] $\eta\rightarrow\gamma\gamma$ is used.
[c] $\eta\rightarrow\pi^+\pi^-\pi^0$ is used.

TABLE II. Branching ratios of D^+ modes relative to $K^-\pi^+\pi^+$. All upper limits are 90% confidence level.

Mode	$\Gamma/\Gamma(K^-\pi^+\pi^+)$
$\phi\pi^+$	$0.077\pm0.011\pm0.005$
$\eta\pi^+$	$0.083\pm0.023\pm0.014$
$\eta'\pi^+$	<0.10
$\eta\rho^+$	<0.13
$\eta'\rho^+$	<0.17
$\phi\rho^+$	<0.16

C. Detection of the $\eta'\pi^+$ mode

In Fig. 6 we show the $\eta'\pi^+$ invariant-mass spectrum for all three η' decay modes studied: namely, $\eta'\to\pi^+\pi^-\eta$, with (a) $\eta\to\gamma\gamma$, and (b) $\eta\to\pi^+\pi^-\pi^0$ and (c) $\eta'\to\rho\gamma$. Again, the shape of the mass spectrum below the D_s mass was studied carefully in the same manner as for the $\eta\pi^+$ decay mode above. The fit allows for a peak at the D^+ mass and takes account of the reflection from the $\eta'\rho^+$ decay mode. Both the shape and the amount of this reflection are obtained in the same way as for the fit described above for the $\eta\rho+$ decay mode. Event yields and efficiencies are given in Table I. The average branching ratio for the three η' final states is $1.20\pm0.15\pm0.18$ times the branching ratio for the decay $\phi\pi^+$.

A clear D^+ signal is observed neither in this mode nor in any mode subsequently considered, and we present 90%-confidence-level upper limits in Table II.

D. Comparison of $\eta\pi^+$ and $\eta'\pi^+$ decay rates with other measurements

Our results for these two modes are compared with other measurements from E691[9], Mark II[10], Mark III [11], NA14/2[12], and ARGUS [13], as listed in Table III.

TABLE III. Recent measurements of $\eta\pi^+$ and $\eta'\pi^+$.

Experiment	$\Gamma(\eta\pi^+)/\Gamma(\phi\pi^+)$	$\Gamma(\eta'\pi^+)/\Gamma(\phi\pi^+)$
CLEO II	$0.54\pm0.09\pm0.06$	$1.20\pm0.15\pm0.11$
E691 [9]	<1.5 at 90% C.L.	<1.3 at 90% C.L.
Mark II [10]	4.0 ± 1.3	6.4 ± 2.8
Mark III [11]	<2.5 at 90% C.L.	<1.9 at 90% C.L.
NA14/2 [12]		$2.5\pm1.0^{+1.5}_{-0.4}$
ARGUS [13]		2.5 ± 0.7

We obtain a much smaller value for the decay into $\eta\pi^+$ than the one measured by Mark II. Our $\eta'\pi^+$ measurement is also much smaller than the Mark II measurements. It is barely consistent with the ARGUS and NA14/2 measurements, but is in agreement with the Mark III and E691 supper limits.

IV. DECAY MODES OF THE D_s^+ CONTAINING ρ^+

We have also searched for decays where the π^+ in the final state is replaced by a ρ^+. The selection criteria are listed in Appendix A.

A. Detection of the $\eta\rho^+$ mode

The $\eta\pi^+\pi^0$ mass spectrum is shown in Fig. 7, for the subsequent decay $\eta\to\gamma\gamma$, and requiring that the $\pi^+\pi^0$ mass be within ±170 MeV of the ρ^+ mass. The peak at the D_s mass contains 158 ± 22 events. Figure 8(a) shows the $\pi^+\pi^0$ mass spectrum for events in the D_s peak (histo-

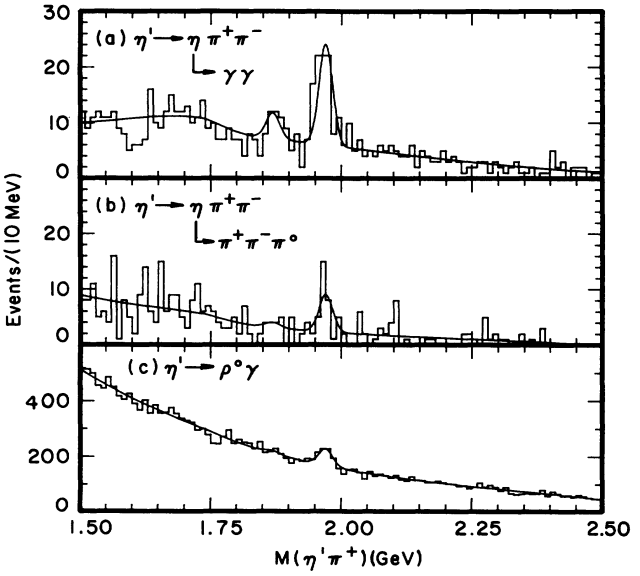

FIG. 6. The $\eta'\pi^+$ invariant-mass spectrum using the $\eta'\to\eta\pi^+\pi^-$ decay mode, for the cases (a) $\eta\to\gamma\gamma$ and (b) $\eta\to\pi^+\pi^-\pi^0$ and for the (c) $\eta'\to\rho^0\gamma$ decay mode. The fits are described in the text.

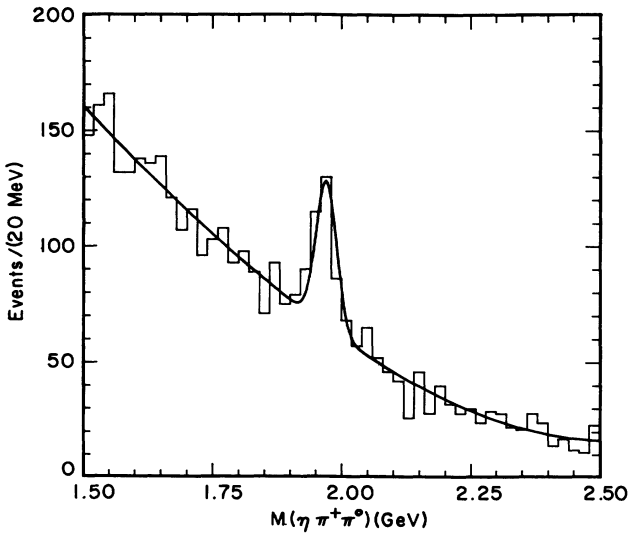

FIG. 7. The $\eta\pi^+\pi^0$ invariant-mass spectrum, for the subsequent decay $\eta\to\gamma\gamma$. The helicity angle requirement $|\cos\theta_{\pi^+}|>0.45$ is imposed, and the invariant mass of the two pions is required to be within ±170 MeV of the ρ^+ mass.

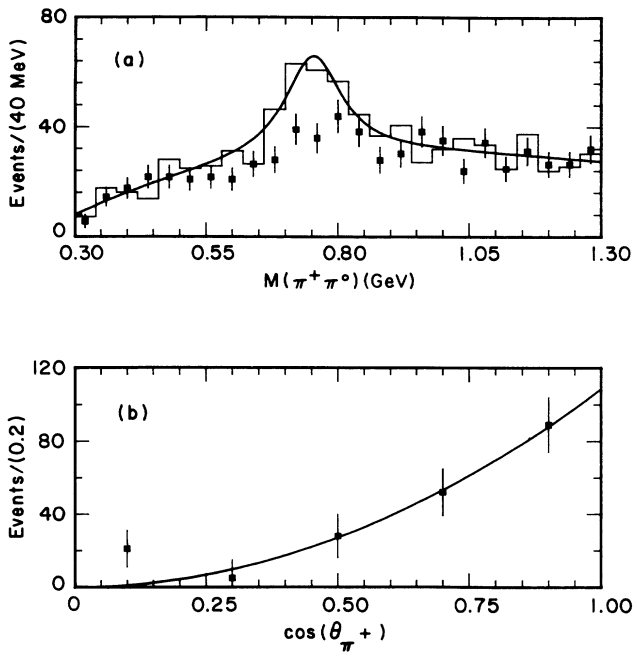

FIG. 8. (a) The $\pi^+\pi^0$ mass spectrum for events in the D_s peak for the $\eta\pi^+\pi^0$ channel (histogram) and sidebands (solid points), both for the case $\eta\to\gamma\gamma$. The helicity angle requirement is still used. (b) The number of D_s events as a function of helicity angle θ_{π^+}. The ρ^+ mass cut is applied. The curve is a fit to the form $\cos^2\theta_{\pi^+}$.

gram) and sidebands (solid points). The peak region is defined as $2.02>M(\eta\pi^+\pi^0)>1.92$ GeV, while the sidebands are comprised of two regions $1.86>M(\eta\pi^+\pi^0)>1.91$ GeV and $2.03>M(\eta\pi^+\pi^0)>2.08$ GeV. The large signal at the ρ^+ mass in the D_s peak region suggests that the $\pi^+\pi^0$ is dominated by ρ^+ [14]. Evidence that the $\pi^+\pi^0$ indeed form a ρ^+ is obtained by removing the helicity angle cut and then, for each θ_{π^+} bin, fitting the number of D_s events above background. This is shown in Fig. 8(b), where the events have been corrected for helicity-dependent efficiencies. The decay chain, $0^-\to1^-0^-$, must have a $\cos^2\theta_{\pi^+}$ distribution. The curve shows the fit of this distribution to the data, the confidence level for the fit being 38%. The isotropic component of distribution can be at most 20% of the signal and this provides an estimate of the nonresonant contribution.

We can however make a more stringent estimate of the maximum amount of nonresonant $\pi^+\pi^0$ by splitting our sample into two regions, one rich in ρ^+ content and the other ρ^+ poor, and then comparing the number of $D_s\to\eta\pi^+\pi^0$ events in these two regions. We assume that the nonresonant component has $\pi^+\pi^0$ mass and $\cos\theta_{\pi^+}$ distributions given by phase space. The ρ-rich region is defined by having the invariant mass of $\pi^+\pi^0$ within ±170 MeV of the ρ^+ mass and $|\cos\theta_{\pi^+}|>0.4$, while the ρ-poor region is defined by not being the ρ-rich region. The relationship between the number of D_s events in the ρ-rich region, N_r, the ρ-poor region, N_p, and the number of nonresonant, events $N_{\rm NR}$ is given by

$$N_p=[N_r-(1-\beta)N_{\rm NR}]\left[\frac{\epsilon'}{1-\epsilon'}\right]+\beta N_{\rm NR}\ , \qquad (1)$$

where ϵ' is the probability that real ρ^+ events fall into the ρ-poor region and β is the fraction of the phase space in the ρ-poor region. Both of these quantities are determined by Monte Carlo simulation. For this decay mode, $\epsilon'=0.24$ and $\beta=0.8$. N_r and N_p are determined by fitting the $\eta\pi^+\pi^0$ invariant-mass spectrum to find the number of D_s events above background. We find N_r and N_p to be 164 ± 23 and 34 ± 30 events, respectively. Solving the equation gives $N_{\rm NR}=-22\pm41$, from which we derive a 90%-confidence-level upper limit of <55 events over all of phase space or <11 events in the ρ-rich region. Thus we find that under the assumption that the non-ρ^+ decay follows phase space, the maximum amount of nonresonant signal in our quoted $\eta\rho^+$ branching ratio is 7% at 90% confidence level.

The results for this decay branching ratio, using $\eta\to\gamma\gamma$ and $\eta\to\pi^+\pi^-\pi^0$ are presented in Table I. The average branching ratio for the two η decay modes is $2.86\pm0.38^{+0.36}_{-0.38}$ times the branching ratio for the $\phi\pi^+$ decay. Included in the negative systematic error is the uncertainty in our estimate of the non-ρ component added in quadrature with the other errors.

We also set an upper limit on the nonresonant decay $D_s^+\to\eta\pi^+\pi^0$ assuming a phase-space distribution, which is given in Table IV.

B. Detection of the $\eta'\rho^+$ mode

For our analysis of the $\eta'\rho^+$ mode, we use only the $\eta'\to\eta\pi^+\pi^-$ decay mode. In the $\eta'\to\rho^0\gamma$ channel there is a large background in the $\eta'\rho^+$ mass plot, which peaks near the D_s mass. The decay chains and cuts are listed in Appendix A. In this final state, the maximum energy available to the dipion system is ~1 GeV, which limits the upper value of dipion phase space to being close to the ρ peak. Since the ρ has a large width, there is some uncertainty in extracting the ρ component of the signal. The $\eta'\pi^+\pi^0$ mass spectrum is shown in Fig. 9 for the case

TABLE IV. Upper limits for nonresonant $\pi^+\pi^0$ decays at 90% confidence level.

Mode	$\Gamma/\Gamma(\phi\pi^+)$	ϵ'	β	N_r	N_p	$N_{\rm NR}$
$\eta\pi^+\pi^0$	0.82	0.24	0.80	164±23	34±30	−22±41
$\eta'\pi^+\pi^0$	0.85	0.18	0.70	59±11	6.3±9.7	−13±13
$\phi\pi^+\pi^0$	0.71	0.0	0.28	253±32	3.3±16.7	12±60

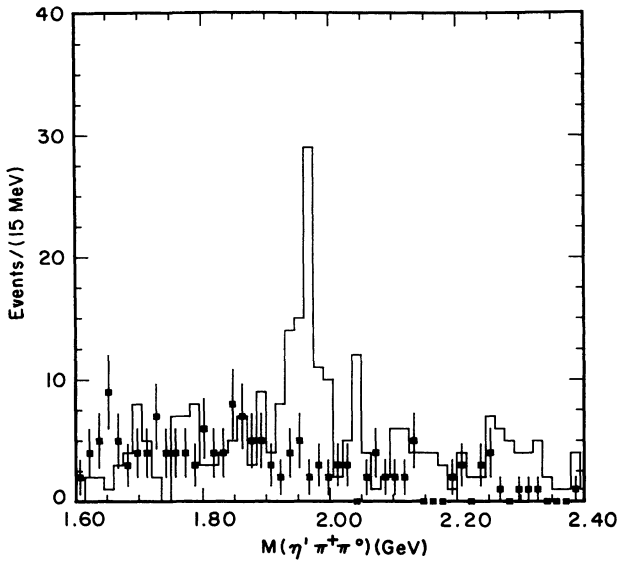

FIG. 9. The $\eta'\pi^+\pi^0$ invariant-mass spectrum, for the decay $\eta'\to\eta\pi^+\pi^-$, with $\eta\to\gamma\gamma$. The ρ^+ mass cut and the helicity angle cut are applied. The solid points are for the lower sideband of the ρ, defined as $\pi^+\pi^0$ masses below 500 MeV.

where the η decays to two photons. The $\pi^+\pi^0$ invariant mass is required to be within ± 170 MeV of 770 MeV. The peak at the D_s mass contains 53 ± 10 events. The distribution shown with solid points was obtained by requiring that the $\pi^+\pi^0$ mass be below 500 MeV. No D_s signal is apparent in this case, thus indicating that the signal is due mostly to the ρ^+. We show in Fig. 10(a) the $\pi^+\pi^0$ mass spectrum for events in the D_s peak (histogram) and D_s sidebands (full points). [The mass intervals are the same as used for Fig. 8(a).] There is peaking in the ρ^+ mass region for the sample from the D_s peak, but not from the D_s sidebands. In Fig. 10(b) we show the helicity angle distribution of the ρ^+ candidates. The fit to the $\cos^2\theta_{\pi^+}$ distribution has a confidence level of 10%. Our data are therefore consistent with the spin-1 hypothesis. Using only the helicity angle we limit the possible contribution of a nonresonant background to at most 20%. To find a more stringent limit we again use Eq. (1) for this decay channel. Since the ρ^+ line shape is modified by the limited phase space available, our evaluation of ϵ' for this channel is affected by the ρ^+ shape we use. As the actual shape depends on the unknown decay matrix element, we use a generous cut on the $\pi^+\pi^-$ invariant mass of ± 170 MeV in order to minimize any possible effect. To evaluate the systematic differences we use several shapes and find that the largest difference within our cut is 4% and we have included this in the systematic uncertainty. The numbers of events are given in Table II. We set an upper limit of $<8\%$ at 90% confidence level on the amount of nonresonant $\pi^+\pi^0$ in the ρ^+ region.

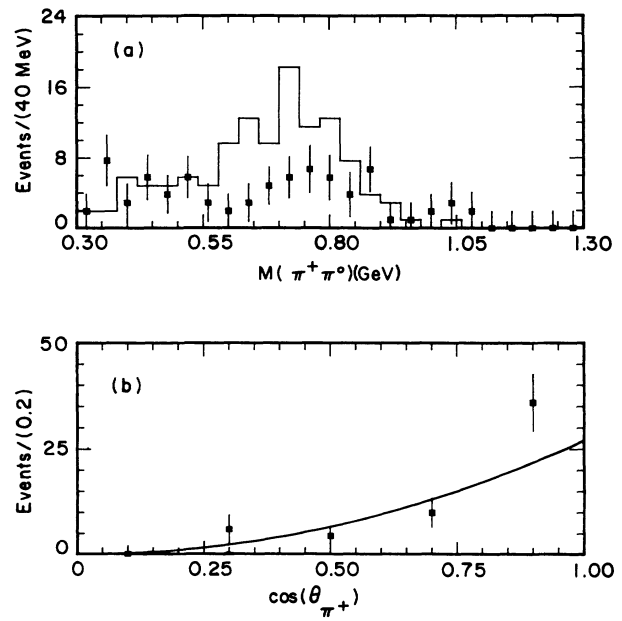

FIG. 10. (a) The $\pi^+\pi^0$ mass spectrum for events in the D_s mass peak in the channel $\eta'\pi^+\pi^0$ and $\eta\to\gamma\gamma$ (histogram) and in the D_s sidebands (solid points). The helicity angle cut is applied. (b) The helicity angle distribution from the ρ^+ band.

The branching ratio for this decay chain, together with a similar analysis for the decay, $\eta'\to\eta\pi^+\pi^-$ with the daughter decay $\eta\to\pi^+\pi^-\pi^0$, is presented in Table I. We find a rather large relative branching ratio (average of the two η decay modes) of $3.44\pm 0.62^{+0.44}_{-0.46}$.

C. Detection of the $\phi\rho^+$ mode

The $\phi\pi^+\pi^0$ mass plot is shown as the histogram in Fig. 11. The $\pi^+\pi^0$ invariant mass is required to be within ± 170 MeV of the ρ^+ mass. The curve is a fit to a two-signal Gaussian with means fixed at the D_s^+ and D^+ masses and fixed widths, the value of the latter being

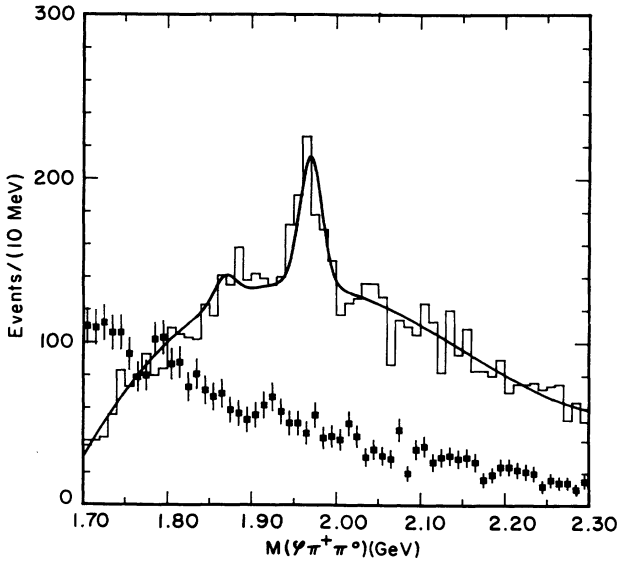

FIG. 11. The $\phi\pi^+\pi^0$ invariant-mass spectrum (histogram) for $\pi^+\pi^0$ invariant masses within ± 170 MeV of the ρ^+ mass. The solid points are for $\pi^+\pi^0$ invariant masses below 500 MeV.

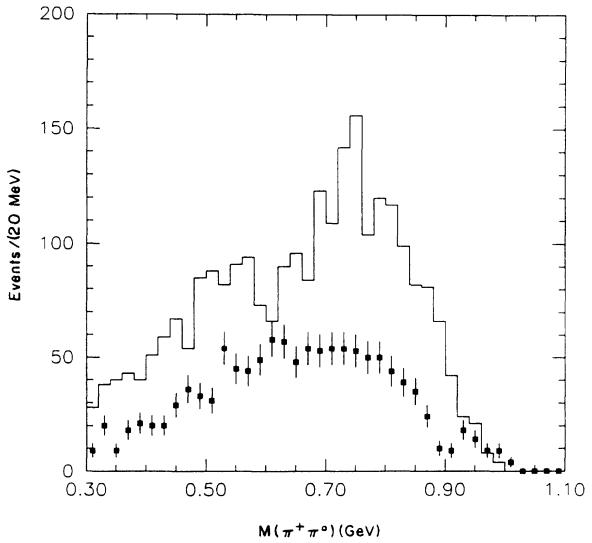

FIG. 12. The $\pi^+\pi^0$ mass spectrum for events in the D_s peak for the $\phi\pi^+\pi^0$ channel (histogram) and sidebands (solid points).

determined from Monte Carlo studies, and a background polynomial. A clear peak with 253±32 events is observed. Also shown is the mass spectrum for events from the lower sideband of the ρ, defined as $\pi^+\pi^0$ masses below 500 MeV (dashed line), which does not show any peaking in the D_s region. Figure 12 shows the $\pi^+\pi^0$ mass spectrum for events in the D_s peak (histogram) and sidebands (solid points). Again the peak region is defined as $2.0025 > M(\phi\pi^+\pi^0) > 1.9375$ GeV, while the sidebands are comprised of two regions $1.9245 > M(\phi\pi^+\pi^0) > 1.892$ GeV and $2.048 > M(\phi\pi^+\pi^0) > 2.0155$ GeV. There is an apparent enhancement at the ρ^+ mass. The background level is approximately half of the signal level because the upper sideband has almost no events due to the lack of phase space.

If we interpret this peak as evidence for D_s decay to the final state $\phi\rho^+$, we find a branching ratio, relative to $\phi\pi^+$, for this decay mode of 1.86±0.26±0.29. Our result is consistent with a previous E691 measurement [9], which was based on a sample of 11±3.6 events.

To ascertain the maximum amount of nonresonant $\pi^+\pi^0$ allowed by the data, we again use Eq. (1); however, in this case, the $\cos\theta_{\pi^+}$ distribution is not predetermined by angular momentum considerations. Therefore, the ρ-rich and ρ-poor regions are defined only in terms of invariant $\pi^+\pi^0$ mass. The ρ-rich region has $\pi^+\pi^0$ invariant mass above 0.6 GeV, while the ρ-poor region has invariant mass below 0.5 GeV. The region between 0.5 and 0.6 GeV is left out of this analysis. The fraction of phase space in the ρ-rich region is 0.56, while $\beta=0.26$. The relevant numbers of events are given in Table II. We find that the upper limit at 90% confidence level on the amount of nonresonant $\pi^+\pi^0$ is $<20\%$. Again, this assumes that the nonresonant part has a phase-space distribution. The final result is given in Table V.

V. COMPARISON WITH THEORY

We compare our results with several models. The model of Bauer, Stech, and Wirbel [15] (BSW) makes definite, parameter-free predictions of the widths relative to $\phi\pi^+$ for the modes we have measured. They use form factors calculated from $q\bar{q}$ wave functions and consider color-allowed and color-suppressed decays. For comparison with the $\eta\pi^+$ and $\eta'\pi^+$ results, Kamal, Sinha, and Sinha [16] (KSS) have modified the BSW results by changing the value of the η-η' mixing angle, Θ, from $-11°$ to the value found by Gilman and Kaufman [17], namely $\Theta=-19°$. BSW used the value, Θ of $-11°$. A more negative mixing angle increases the decay rates to the η' modes and reduces those to the η modes. KSS also make predictions using their own model in which the form factors are found from SU(4) symmetry. We also include predictions from QCD sum rules, as determined by Blok and Shifman [18] (BS). In Table V we compare our results with these models.

The discrepancy with the BSW theory for the vector-vector decay state $\phi\rho^+$ may be related to the small form factors observed in the semileptonic decay $D\to K^* l\nu$ [19]. Overall, these theories do not give good agreement with our results.

VI. FRACTION OF KNOWN D_s DECAYS

A. The $\phi\pi^+$ absolute branching ratio

It is possible to estimate the absolute branching ratio for any D_s decay mode, by first measuring the ratio of the decay width of this mode relative to the width of the $\phi l^+\nu$ mode. The width for the decay $\phi l^+\nu$ is $\mathcal{F}$ times the width of the decay $D\to K^* l^+\nu$, where $\mathcal{F}$ is given by theory, as discussed below. The procedure is to measure the ratio $\mathcal{B}(D_s\to\phi l^+\nu)/\mathcal{B}(D_s\to\phi\pi^+)$ and then to obtain $\mathcal{B}(D_s\to\phi l^+\nu)$ from the formula

TABLE V. Relative branching ratios compared with theory.

Mode	$\Gamma/\Gamma(\phi\pi^+)$ This experiment	BSW	$\Gamma/\Gamma(\phi\pi^+)$ theory BSW,$\Theta=-19°$	KSS	BS
$\phi\pi^+$	1	1	1	1	1
$\eta\pi^+$	0.54±0.09±0.06	1.04	0.75	1.35	1.13
$\eta'\pi^+$	1.20±0.15±0.11	0.61	0.78	1.47	0.10
$\eta\rho^+$	$2.86\pm0.38^{+0.36}_{-0.38}$	1.96			2.33
$\eta'\rho^+$	$3.44\pm0.62^{+0.44}_{-0.46}$	0.56			
$\phi\rho^+$	$1.86\pm0.26^{+0.29}_{-0.40}$	6.30			

TABLE VI. Well-established D_s branching ratios [2].

Decay mode	Branching ratio relative to $\phi\pi^+$
$\phi\pi^+$	1
$\bar{K}^0K^+$	0.97±0.17
$\bar{K}^{*+}\bar{K}^0$	1.2±0.25
$\bar{K}^{*0}K^+$	0.96±0.11
$\bar{K}^{*+}K^{*+}$ [30]	1.6±0.6
$(K^-K^+\pi^+)_{NR}$	0.25±0.09
$\phi\pi^-\pi^+\pi^+$	0.48±0.20
$f_0(975)\pi^+$	0.28±0.10
$(\pi^-\pi^+\pi^+)_{NR}$	0.29±0.09

$$\mathcal{B}(D_s\to\phi l^+\nu)=\mathcal{F}\cdot\mathcal{B}(D^+\to K^{*0}l^+\nu)\frac{\tau_{D_s}}{\tau_{D^+}}\ .$$

There is, however some uncertainty among the models used. In particular, using the model of Isgur *et al.* [20], Scora has recently predicted [21] that $\mathcal{F}=1.02$, which differs considerably from the value of 0.78 previously used for this model. The value in the WBS model remains as 0.83 [22]. Here, we use the average value of $\mathcal{F}$ from these two models. Using the well-measured ratio of lifetimes [2] 0.42±0.03 and the $K^{*0}l^+\nu$ branching-ratio average value of (4.8±0.9)% from E691 [23], ARGUS [4], WA82 [24], and Mark III [25,26], we estimate $\mathcal{B}(D_s\to\phi l^+\nu)=(1.9\pm0.4)\%$

There have been two measurements of $\mathcal{B}(D_s\to\phi l^+\nu)/\mathcal{B}(D_s\to\phi\pi^+)$. CLEO [3] obtained the result $0.49\pm0.10^{+0.10}_{-0.14}$ and ARGUS [4] the result $0.57\pm0.15\pm0.15$ [27]. Averaging these two results yields the value of $\mathcal{B}(D_s\to\phi\pi^+)$ of (3.7±1.2)%.

B. The semileptonic branching ratio

Assuming that the semileptonic widths of charmed mesons are equal as evidenced by the equality within experimental errors of the D^0 and D^+ semileptonic widths, and using the well-measured charmed-meson lifetimes [2], estimate that $\mathcal{B}(D_s\to Xe^+\nu)=(8\pm1)\%$ [28].

In addition, there are estimates of the purely leptonic branching ratio $\mathcal{B}(D_s^+\to\tau^+\nu+\mu^+\nu)\approx2$–5 % [29], but as this contribution is not measured, we do not include it in the sum.

C. Sum of known branching ratios

The sum of widths of the modes measured in this paper relative to $\phi\pi^+$ is 9.9±0.8±0.7. In addition, the well-established decay modes are shown in Table VI. We have included a recent result from ARGUS for the $\bar{K}^{*0}K^{*+}$ mode [30]. These sum up to 7.0±0.7 times $\phi\pi^+$ [31].

Thus the sum of measured hadronic modes is 16.9±1.3 times the $\phi\pi^+$ branching ratio. The sum of all known decay modes is 8% (semileptonic decay to electrons), plus 8% (semileptonic decay to muons), plus (63±26)% (hadronic decay). This gives a total of ≈(79±26)%, where the error is dominated by the error on the $D_s\to\phi\pi$ branching ratio.

VII. CONCLUSIONS

We have measured the branching ratios, relative to the $\phi\pi^+$ mode, of a large fraction of the hadronic D_s^+ decay modes. The $\eta\pi^+$ and $\eta'\pi^+$ modes have significantly smaller branching ratios than previously reported. The $\eta\rho^+$ and $\eta'\rho^+$ modes have been seen for the first time and the $\phi\rho^+$ has been confirmed. The latter decay modes have significantly larger rates than the $\phi\pi^+$ mode. The $\eta'\pi(\rho)$ modes are larger than the corresponding $\eta\pi(\rho)$ modes. Current theoretical models do not give a good description of these results.

TABLE VII. Cuts used in forming D_s candidates.

Mode	$s\bar{s}$ decay (ϕ,η,η')	Momentum (GeV)	Mass[a] (MeV)	Helicity angle	Decay angle
$\phi\pi^+$	K^+K^-		±8	$\lvert\cos\theta_{K^+}\rvert>0.45$	$\cos\alpha_\phi<0.8$
$\eta\pi^+$	$\gamma\gamma$		±35[b]		$\lvert\cos\alpha_\eta\rvert<0.8$
	$\pi^+\pi^-\pi^0$	$P_{\pi^0}>0.3$	±15		$\lvert\cos\alpha_\eta\rvert<0.8$
$\eta'\pi^+$	$\eta\pi^+\pi^-$	$P_\eta>0.3$	±15, ±23		$\lvert\cos\alpha_{\eta'}\rvert<0.8$
	$\rho^0\gamma$	$P_\gamma>0.1$	±28	$\lvert\cos\theta_{\pi^+}\rvert<0.8$	$\lvert\cos\alpha_{\eta'}\rvert<0.8$[c]
$\eta\rho$[d]	$\gamma\gamma$	$P_{\pi^0}>0.3$	±35[b]	$\lvert\cos\theta_{\pi^+}\rvert>0.45$	$\lvert\cos\alpha_{\rho^+}\rvert<0.8$
	$\pi^+\pi^-\pi^0$	$P_{\pi^0}>0.3$[e]	±15	$\lvert\cos\theta_{\pi^+}\rvert>0.45$	$\lvert\cos\alpha_{\rho^+}\rvert<0.8$
$\eta'\rho^+$[d]	$\eta\pi^+\pi^-$	$P_\eta>0.3$	±15, ±23	$\lvert\cos\theta_{\pi^+}\rvert>0.45$	$\lvert\cos\alpha_{\rho^+}\rvert<0.8$
$\phi\rho^+$[d]	K^+K^-	$P_{\pi^0}>0.3$	±8		

[a]Mass cut on the primary $s\bar{s}$ system. Where two numbers are presented, the first applies to the $\eta\to\gamma\gamma$ mode, and the second to the $\eta\to\pi^+\pi^-\pi^0$ mode.
[b]The mass cut varies from 34 to 37 MeV as $P_{\gamma\gamma}$ increases.
[c]In addition, the γ direction in the η' rest frame is required to have $\cos\alpha_\gamma>-0.5$.
[d]The ρ^+ mass cut is ±170 MeV.
[e]Applies to the both the π^0 from the ρ^+ decay and the π^0 from the η decay.

TABLE VIII. Checks of Monte Carlo efficiencies.

Ratio	Our measurement	"Known" result
$\Gamma(\eta\to\gamma\gamma)/\Gamma(\eta\to\pi^+\pi^-\pi^0)$	1.66±0.03±0.07	1.64±0.04
$\Gamma(D^0\to K^-\pi^+\pi^0)/\Gamma(D^0\to K^-\pi^+)$	3.0±0.1±0.2	3.2±0.3
$\Gamma(D^{*+}\to D^+\pi^0)/\Gamma(D^{*+}\to D^0\pi^+)$[a]	0.45±0.03±0.09	0.45±0.04

[a] $D^+\to K^-\pi^+\pi^+\pi^0$, $D^0\to K^-\pi^+$.

ACKNOWLEDGMENTS

We gratefully acknowledge the effort of the CESR staff in providing us with excellent luminosity and running conditions. We thank BDH Ltd. (now called Merck Ltd.), Poole, England and Horiba Ltd., Kyoto, Japan, for their superb efforts in manufacturing high-quality crystals for the CLEO II detector. P.S.D. thanks the PYI program of the NSF, K.H. thanks the Alexander von Humbolt Stiftung Foundation, G.E. thanks the Heisenberg Foundation, and R.P. and P. Rankin thank the A.P. Sloan foundation for support. This work was supported by the National Science Foundation and the U.S. Department of Energy.

APPENDIX A: SELECTION CRITERIA

The mass cuts, decay angle cuts, and helicity angle cuts for different D_s modes are listed in Table VII. In the case of $\eta'\pi^+$, with the η' decaying into $\rho^0\gamma$, the ρ^0 is polarized as $\sin^2\theta_{\pi^+}$. The minimum momentum cuts, imposed on some particles to reduce backgrounds, are listed.

APPENDIX B: CHECKS OF RELATIVE MONTE CARLO EFFICIENCIES

Since a measurement of relative branching ratios depends on knowing the relative charged-particle and photon efficiencies, we have performed three checks on our Monte Carlo efficiencies. We measured relative branching ratios of different particle decays and compared our result either with well-established results, or in one case, with the results of isospin invariance. In Table VIII we list the various relative branching ratios that we have measured. The first error quoted is statistical and the second systematic. For D^0 decays we required the D^0 candidate events to come from D^{*+} decay. In the case of the charged D^{*+} test, isospin invariance times phase space is used to give the "known" ratio, and the error is determined from the error on the measured masses, which, in turn, determines the phase-space error.

We conclude that the error is $\approx\pm 7\%$, in our relative efficiencies.

[1] CLEO Collaboration, A. Chen *et al.*, Phys. Rev. Lett. **51**, 634 (1983).

[2] Particle Data Group, J. J. Hernández *et al.*, Phys. Lett. B **239**, 1 (1990).

[3] CLEO Collaboration, J. Alexander *et al.*, Phys. Rev. Lett. **65**, 1531 (1990).

[4] ARGUS Collaboration, H. Albrecht *et al.*, Phys. Lett. B **255**, 634 (1991).

[5] The crystals were manufactured by BDH Ltd., Poole, England (now called Merck Ltd.) and Horiba Ltd., Kyoto, Japan.

[6] E. Blucher *et al.*, Nucl. Instrum. Methods A **249**, 201 (1986); C. Bebek *et al.*, *ibid.* **265**, 258 (1988); the crystal calibration is described in R. Morrison *et al.*, Phys. Rev. Lett. **67**, 1696 (1991).

[7] G. Fox and S. Wolfram, Phys. Rev. Lett. **41**, 1581 (1978).

[8] We use the dipole matrix element to evaluate the shape of the $\pi^+\pi^-$ mass spectrum. See M. Althoff *et al.*, Phys. Lett. **147B**, 487 (1984), and references contained therein.

[9] For $\eta\pi^+$, E691 Collaboration, J. C. Anjos *et al.*, Phys. Lett. B **223**, 267 (1989); for $\eta'\pi^+$, Phys. Rev. D **43**, R2063 (1991).

[10] Mark II Collaboration, G. Wormser *et al.*, Phys. Rev. Lett. **61**, 1057 (1988).

[11] Mark III Collaboration, P. Kim, in *Heavy Quark Physics,* edited by P. Drell and D. Rubin (AIP, New York, 1989).

[12] NA14/2 Collaboration, M. P. Alvarez *et al.*, Phys. Lett. B **255**, 639 (1991).

[13] ARGUS Collaboration, H. Albrecht *et al.*, Phys. Lett. B **245**, 315 (1990).

[14] The data in the D_s fit well to a Breit-Wigner form for the ρ plus background, giving 204±57 events. This number is somewhat larger than the number quoted (158) for $\eta\rho^+$ above and given in Table I, because the latter has not been corrected for the ρ mass cut of ±170 MeV and there is possibly some ρ^+ signal from the $\eta\pi^+\pi^0$ background below the D_s peak.

[15] M. Bauer, B. Stech, and M. Wirbel, Z. Phys. C **34**, 103 (1987).

[16] A. N. Kamal, N. Sinha, and R. Sinha, Phys. Rev. D **38**, 1612 (1988).

[17] F. J. Gilman and R. Kauffman, Phys. Rev. D **36**, 2761 (1987).

[18] B. Yu. Blok and M. A. Shifman, Yad. Fiz. [Sov. J. Nucl. Phys. **45**, 522 (1987)].

[19] E691 Collaboration, J. C. Anjos *et al.*, Phys. Rev. Lett. **65**, 2630 (1990).

[20] N. Isgur, D. Scora, B. Grinstein, and M. B. Wise, Phys. Rev. D **39**, 799 (1989).

[21] D. Scora, in *Particles and Nuclei,* Proceedings of the Twelfth International Conference, Cambridge, Massachusetts, 1990, edited by J. L. Matthews *et al.* (North-Holland, Amsterdam, 1991).

[22] M. Wirbel *et al.*, Z. Phys. C **29**, 269 (1985).

[23] E691 Collaboration, J. C. Anjos *et al.*, Phys. Rev. Lett. **62**, 722 (1989).

[24] WA82 Collaboration, M. Adamovich *et al.*, Phys. Lett. B **268**, 142 (1991).

[25] Mark III Collaboration, Z. Bai *et al.*, Phys. Rev. Lett. **66**, 1011 (1991); we have used the results of Fit (1) and an analysis of J. Izen (private communication) to extract the K^* fraction.

[26] The E691, ARGUS, and WA82 results are normalized to the absolute $D^+ \to K^- \pi^+ \pi^+$ branching ratio from Mark III as given by the Mark III Collaboration, J. Adler *et al.*, Phys. Rev. Lett. **60**, 89 (1988).

[27] There is also an upper limit of <0.45 at the 90% confidence level from E691. See E691 Collaboration, J. C. Anjos *et al.*, Phys. Rev. Lett. **64**, 2885 (1990). ARGUS has also compared partially reconstructed with fully reconstructed $\bar{B}^0 \to D^{*+} D_s^{*+}$ decays to measure $\mathcal{B}(D_s \to \phi\pi^+) = (1.4 \pm 0.7 \pm 0.4)\%$. See H. Albrecht *et al.*, DESY Report No. 90-157 (unpublished).

[28] This is consistent with the Mark III upper limit of $<25\%$ at 90% C.L., see Z. Bai *et al.*, Phys. Rev. Lett. **65**, 686 (1990).

[29] J. L. Rosner, Phys. Rev. D **42**, 3107 (1990), and references contained therein.

[30] ARGUS Collaboration, H. Albrecht *et al.*, Z. Phys. C **53**, 361 (1992).

[31] The large size of the modes we have measured with respect to the modes having kaons is consistent with the observation that the fraction of D_s decays which do not include kaons is $(64 \pm 17 \pm 3)\%$ from D. Coffman *et al.*, Phys. Lett. B **262**, 135 (1991).